REDUCTION OF DYNAMIC MULTIPOLE CONTENT IN INSERTION DEVICES USING FLAT WIRES*

T.Y. Chung†, S.J. Huang, M.S. Chiu, C.Y. Kuo, S.D. Chen, C.Y. Wu, Y.T. Li, J.C. Jan and C.S. Hwang,
National Synchrotron Radiation Research Center, Hsinchu, Taiwan

Abstract

Multipole errors of an insertion device are generally corrected based on measurements and analysis of the magnetic field integrals. Multipole components in a strong and narrow non-uniform field of an insertion device appear as dynamic multipoles. Flat wires were installed and commissioned to determine if the dynamic multipoles can be eliminated in an APPLE-II type undulator. In this work, we will discuss and compare the reduction of the dynamic multipole content and its beam dynamics effects with the flat wire through an analysis of field calculations and beam-based measurements in the storage ring.

INTRODUCTION

The magnetic field of accelerator magnets, like a quadrupole or a sextupole, usually can be described by a cylindrical multipole expansion [1] about their axes. The static field integral along its straight axis is measured by a rotating coil or a stretched wire. The same measurement and analysis method is also commonly performed on insertion devices (ID). The field distribution in the accelerator magnet along its longitudinal axis is invariant except for the end fields and can be described by a two dimensional magnetic field expansion. The field in an ID, however, changes periodically, and the field integral does not directly expose variations of the peak field but only the integral of all fields. In other words, it is possible to have a uniform distribution of the field integral while the field amplitudes vary with horizontal displacements. The electron beam, passing through an ID, will, however, react to all fields along its path, be it uniform or not. The common method to characterize an ID by a straight field integral is therefore not sufficient.

A narrow wiggler pole width can affect both linear focusing and nonlinear transverse dynamics [2] due to the rapid transverse field roll-off combined with the wiggling motion of an electron beam creating a dynamic field integral along the particle path being proportional to the square of the magnetic field and the length of an ID [3]. Unlike a typical ID, the APPLE-II type undulator has four Halbach arrays that are horizontally separated to allow their symmetric or antisymmetric movement [4]. The transverse roll-off of the vertical fields is therefore significant and especially the horizontal field of an APPLE-II shows an inherently rapid transverse roll-off. For a universal operation of the APPLE-II, beam dynamic effects have been studied using particle tracking [5,6].

To minimize multipole errors in the dynamic field integral, passive corrective methods exist, e.g. in the form of L-shaped iron shims attached to the corners of the magnet blocks [7-9] or active methods like flat current wires glued onto the undulator vacuum chamber [10-12] as proposed and implemented. The degree of correction is to be guided by the dynamic field integral representing the effective multipole influence on the electron beam. It should be noted that the passive method is convenient but inaccurate for an inclined mode of the APPLE-II and operation of the storage ring at different energies.

The APPLE-II has become the work-horse in the Taiwan Light Source (TLS) and the Taiwan Photon Source (TPS) to produce circular polarized synchrotron radiation. To assure stable operation, we continue to study beam dynamic effects induced by the EPU56 (period length: 56 mm) operating in the TLS at 1.5 GeV. In our previous observations, the dynamic field integral and the beam size variations were compensated by L-shaped iron shims and by multipole magnets in the ring, respectively [13]. To be stable for universal operation, a flat wire was installed and tested at the TLS during the 2017 summer shutdown. The installation of the flat wire could be completed without disturbing the position of the EPU56 and existing vacuum chamber even though it was glued to the chamber inside the EPU56 gap. To achieve this difficult installation, a complete installation test was performed on a measurement bench. Considerations for installation and commissioning are discussed below.

This paper is organized as follows. In Section 2, we discuss the strategy to compensate the dynamic field integral and beam size variation. In Section 3, the tests on the measurement bench and considerations for the installation will be discussed. In Section 4, commissioning results and effects on the beam dynamics will be discussed. A summary is given in Section 5.

THEORETIC BACKGROUND AND SIMULATION

The undulator-induced effects are analysed based on the expansion of the deflecting angles of an electron passing through an undulator [3],

$$\theta_{x,y}(L) = \theta_{x,y}(0) \pm \frac{e}{\gamma m_0 C} \int_0^L B_{y,x} ds - \frac{1}{2}\left(\frac{e}{\gamma m_0 C}\right)^2 \int_0^L \frac{\partial \Phi}{\partial x,y} ds + O\left(\frac{1}{\gamma^3}\right) \tag{1}$$

The undulator extends from 0 to L, $\theta_{x,y}(L)$ is the horizontal/vertical deflecting angle, γ is the Lorentz factor, $e/\gamma m_0 C$ is the inverse magnetic rigidity, Φ is the magnetic

02 Photon Sources and Electron Accelerators

T15 Undulators and Wigglers

potential. The "+" and "-" is used for the horizontal deflecting angle (HDA) and the vertical deflecting angle (VDA), respectively, while the first term is the entry angle. The second term is the first-order field integral in terms of $1/\gamma$, also known as the static field integral. The integral depends on the transverse coordinates, and represents thus static multipoles. The third term is second-order in $1/\gamma$ and proportional to the square of the magnetic field and the length of the undulator; compared with the static field integral, the third term comes from the integral of the magnetic field along the wiggling electron trajectory, which is the definition of the dynamic field integral. It cannot be measured along a straight line, but must be derived from the potential Φ, which can be determined with numerical codes such as Radia [14].

Beam-dynamic effects of an ID can be alternatively expressed in terms of a betatron tune shift,

$$\begin{bmatrix} d\nu_x & \kappa_{xy} \\ \kappa_{yx} & d\nu_y \end{bmatrix} \approx \frac{1}{4\pi} \begin{bmatrix} \frac{\partial}{\partial x} & \frac{\partial}{\partial x} \\ \frac{\partial}{\partial y} & \frac{\partial}{\partial y} \end{bmatrix} \begin{bmatrix} \overline{\beta_x}\,\theta_x(L) \\ \overline{\beta_y}\,\theta_y(L) \end{bmatrix} \qquad (2)$$

where $d\nu_{x,y}$ is the horizontal/vertical tune shift, $\kappa_{xy,yx}$ is related to the betatron coupling and $\overline{\beta_{x,y}}$ is the average value of the horizontal or vertical beta function over the length of the ID. It should be noted that a horizontal gradient of the HDA generates a horizontal tune shift. A similar result is observed in the vertical component. The cross terms give rise to coupling effects. In other words, if we want to reduce the tune shift, the gradient of the deflecting angle in the corresponding direction must be minimized. To decrease the coupling, the gradient of the deflecting angle in the other direction must be decreased. For correction, the electron beam experiences a magnetic field generated by the flat wire modifying the deflecting angles.
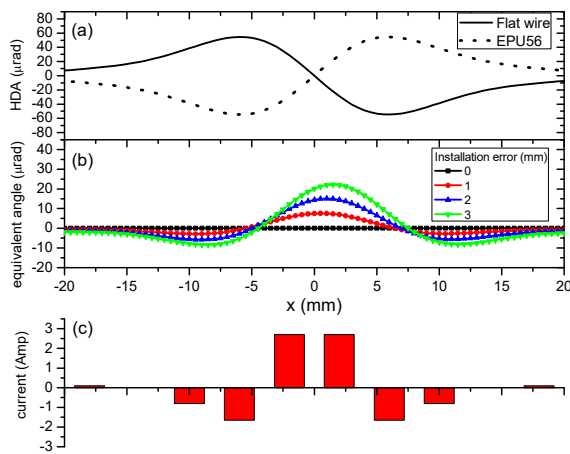

Figure 1: (a) Horizontal distribution of the HDA as contributed by the flat wire (solid) and the EPU56 (dot). (b) Equivalent angles for four installation conditions. (c) Power supply current settings for the EPU56 with a gap of 21.5 mm and a phase of 28 mm.

According to Eq. (1), the exit angle of the electron beam can be modulated using the flat wire. Figure 1(a) shows the horizontal distribution of the HDA in the EPU56 for vertical linear modes (phase = 28 mm). According to Eq. (2), the slope causes an obvious horizontal tune shift, which can be compensated by an inverse HDA introduced by the flat wire, as indicated by the solid line in Fig. 1(a). In this case, the current setting has a maximum value of less than 3 A and presents a mirror symmetry with respect to the axis of the electron beam, as seen in Fig. 1(c). The combination of the flat wire and EPU56 lead to a negligible HDA. Otherwise, installation errors, for example a horizontal offset corresponding to the electron beam axis, induce a dipole angle, as seen in Fig. 1(b).

PRE-INSTALLATION TEST AND INSTALLATION

To achieve the installation of the flat wire on the existing chamber in the tunnel during a short shutdown, a test was performed on a dummy chamber on the measurement bench, as seen in Fig. 2(a). A stretched wire system is set up to measure the integral field as a test of the power supply system and installation process. The critical installation in the tunnel was completed as shown in Fig. 2(b). An alignment tolerance of 0.1 mm, corresponding to a dipole deflection angle of ~0.7 μrad, was achieved using a laser tracker.

Before commissioning in the ring, a temperature measurement on the flat wire was performed. The concern was that the heat created by the exciting current in the flat wire would transfer to the permanent NdFeB magnet which has a high temperature coefficient. A direct temperature measurement on the magnet surface is however difficult to do at the minimum gap. Alternatively, a thermal simulation analysis based on temperature measurements on the surface of the flat wire was pursued. Although the maximum current during operation is less than 3 A, the simulation was done for a heat load at the power supply limit of 10 A. The temperature measurements are shown in Fig. 2(c) and were recorded over time as seen in Fig. 3. The temperature on the flat wire increases by about 2 degrees. Due to the vacuum chamber cooling channel, simulations show, that the magnet surface temperature increased by only 0.1 degree, as shown in the Fig. 3 inset.
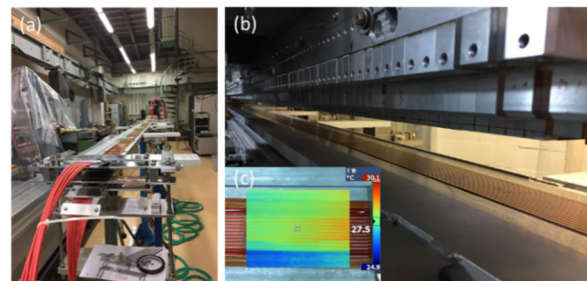

Figure 2: (a) Tests on the measurement bench. (b) Photo of the flat wire installed on the chamber within the gap of the EPU56. (c) Photo of temperature measurements using a thermal imager. The measurement was performed with a

This is a preprint — the final version is published with IOP

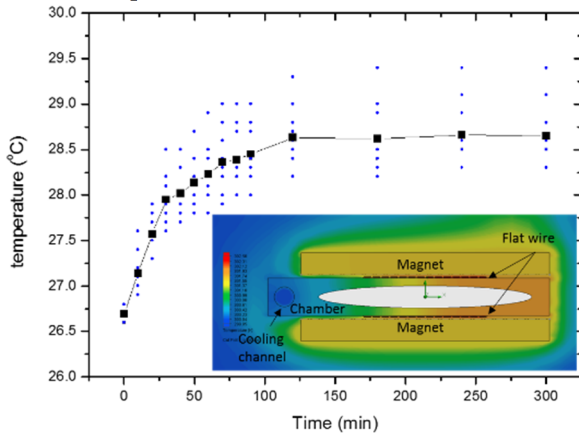current of 10 A, which is three times larger than the maximum operational value.

Figure 3: Temperature measurements versus time on the flat wire with 10 A. The insert shows the thermal simulation analysis in the minimum gap of the EPU56.

COMMISSIONING IN THE RING

Before commissioning in the ring, a table of the current settings as a function of gap and phase was compiled using the simulation process described in Section 2. Following the table, fine tuning allowed to maintain ring parameters like horizontal and vertical tune shifts, beam sizes and injection efficiency constant while changing phase and gap of the EPU56. Figure 4 shows archived data from the commissioning when the current was turned on and off, which is indicated in Fig. 4(a). The ring parameters varied obviously with changes of the phase, especially at the phase of 28 mm. We can see in Fig. 4 that the horizontal/vertical tune shifts of -18.6/4 kHz and the horizontal/vertical beam size variations of -0.8/5.3 µm at the phase of 28 mm were minimized when the flat wire was turned on.
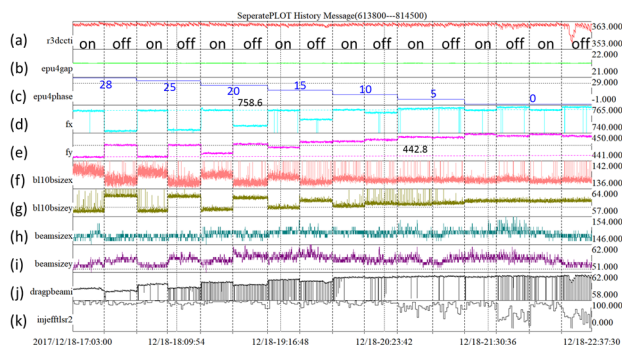

Figure 4: (a) Beam current, (b) gap, (c) phase, (d) horizontal (e) vertical tune shift, (f) horizontal and (g) vertical beam size at bl10, (h) horizontal and (i) vertical beam size at R1BM3, (j) photon intensity and (k) injection efficiency.

Detailed effects of the flat wire on tune shifts and beam sizes are shown in Figs. 5 and 6, respectively. The effects of the EPU56 without compensation show that a negative horizontal tune shift at the phase of 28 mm becomes smaller and changes sign with a change of the phase toward zero. The vertical tune shift, however, is always positive. Compensating the horizontal tune shift with the flat wire works well but not for the vertical tune shift and is even worse in the region with a phase of ±9 mm, as seen by the solid symbols in Fig. 5. The reason is that the contribution to the tune shifts from the flat wire is of opposite sign in the horizontal and vertical plane. If both need compensation with the same sign such as in the region of the phase of ±9 mm, a compromise must be made. In other words, a flat wire with the present current distribution cannot focus or defocus the electron beam at the same time in both directions without contributing to the cross term in Eq. (2) for beam size modulation. A slight current tuning to cause a non-mirror symmetry was performed here to correct the tune shifts as well as beam sizes. As for the growth of the vertical beam size, a maximum of 8% occurs at the phase of 28 mm without compensation which then can be reduced to ~1% with a flat wire correction, as seen in Fig. 6. Although the compensation works well at the phase of 28 mm, it still needs a better optimization for other phases.
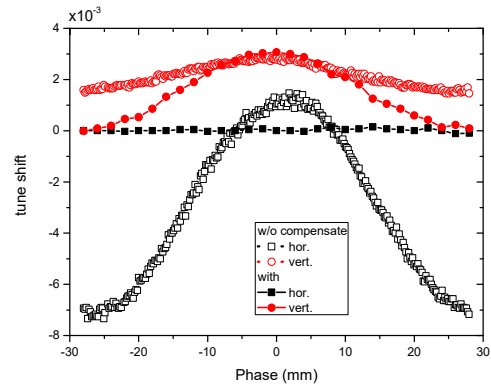

Figure 5: Horizontal and vertical tune shifts as a function of the phase for a wire current turned on and off.
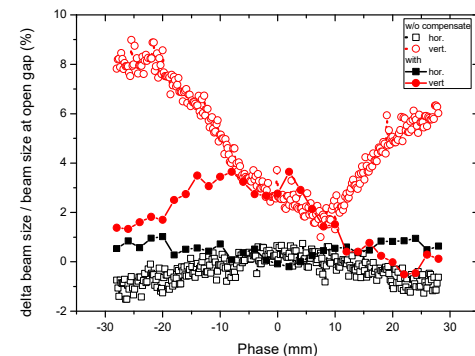

Figure 6: Horizontal and vertical beam sizes as a function of the phase for the wire current turned on and off.

DISCUSSION

The work describes the improvement on multipole errors induced by an undulator using a flat wire. Following theoretical simulations and pre-installation tests, installation and commissioning could be accomplished. The improved ring stability is experimentally evident, but

the present strategy for multi-objective optimization needs more developments.

REFERENCES

[1] A.K. Jain, Basic Theory of Magnets, CERN Accelerator School, 1997.

[2] J. Safranek *et al.*, *Phys. Rev. Accel. Beams 5*, 010701 (2002).

[3] P. Elleaume, in *Proc. EPAC 1992*, Berlin, Germany, pp. 661–3.

[4] S. Sasaki, *Nucl. Instrum. Methods Phys. Res.*, Sect. A 347, 86 (1994).

[5] J. Bahrdt, and G. Wustefeld, *Phys. Rev. ST Accel. Beams 14*, 040703 (2011).

[6] W. Wurtz, D. Bertwistle and M. Sigrist, in *proc. IPAC 2014*, Dresden, Germany, pp. 1995–7.

[7] J. Chavanne *et al.*, in *proc. EPAC 2000*, Vienna, Austria, pp. 2346–8.

[8] J. Bahrdt *et al.*, in *proc. PAC 2007*, Albuquerque, New Mexico, USA, pp. 941–3.

[9] D. Bertwistle *et al.*, in *proc. AIP Conference,* 1741, 020012 (2016).

[10] J. Bahrdt *et al.*, in *proc. EPAC 2008*, Genoa, Italy, pp. 2222–4.

[11] B. Singh *et al.*, in *proc. IPAC 2013*, Shanghai, China, pp. 1997-99.

[12] T. Tanabe *et al.*, *J. Phys.: Conf. Ser.* 493 012031 (2014).

[13] T.Y. Chung *et.al., Nucl. Instrum. Methods Phys. Res.*, Sect. A, 826, 48 (2016).

[14] O. Chubar, P. Elleaume, J. Chavanne, Synchrotron Radiat., 5, 481 (1998).

This is a preprint — the final version is published with IOP